ASCA Observations of "Type 2" LINERs: Evidence for a Stellar Source of Ionization

Yuichi Terashima

NASA Goddard Space Flight Center, Code 662, Greenbelt, MD 20771

Luis C. Ho

Carnegie Observatories, 813 Santa Barbara St. Pasadena, CA 91101-1292

Andrew F. Ptak

Department of Physics, Carnegie Mellon University, 5000 Forbes Ave., Pittsburgh, PA 15213

Richard F. Mushotzky, Peter J. Serlemitsos, and Tahir Yaqoob [1]

NASA Goddard Space Flight Center, Code 662, Greenbelt, MD 20771

and

Hideyo Kunieda[2]

Department of Physics, Nagoya University, Chikusa-ku, Nagoya, 464-8602, Japan

ABSTRACT

We present *ASCA* observations of LINERs without broad Hα emission in their optical spectra. The sample of "type 2" LINERs consists of NGC 404, 4111, 4192, 4457, and 4569. We have detected X-ray emission from all the objects except for NGC 404; among the detected objects are two so-called transition objects (NGC 4192 and NGC 4569), which have been postulated to be composite nuclei having both an H II region and a LINER component.

The images of NGC 4111 and NGC 4569 in the soft (0.5–2 keV) and hard (2–7 keV) X-ray bands are extended on scales of several kpc. The X-ray spectra of NGC 4111, NGC 4457 and NGC 4569 are well fitted by a two-component model that consists of soft thermal emission with $kT \sim 0.65$ keV and a hard component represented by a power law (photon index $\sim$ 2) or by thermal bremsstrahlung emission ($kT \sim$ several keV). The extended hard X-rays probably come from discrete sources, while the soft emission most likely originates from hot gas produced by active star formation in

---

[1] Universities Space Research Association.

[2] present address: Institute of Space and Astronautical Science, Yoshinodai 3-1-1, Sagamihara, Kanagawa 229-8510, Japan

the host galaxy. We have found no clear evidence for the presence of active galactic nuclei (AGNs) in the sample. Using black hole masses estimated from host galaxy bulge luminosities, we obtain an upper limit on the implied Eddington ratios less than 5×10^{-5}. If an AGN component is the primary ionization source of the optical emission lines, then it must be heavily obscured with a column density significantly larger than 10^{23} cm^{-2}, since the observed X-ray luminosity is insufficient to drive the luminosities of the optical emission lines. Alternatively, the optical emission could be ionized by a population of exceptionally hot stars. This interpretation is consistent with the small [O I] $\lambda6300$/Hα ratios observed in these sources, the ultraviolet spectral characteristics in the cases where such information exists, and the X-ray results reported here.

We also analyze the X-ray properties of NGC 4117, a low-luminosity Seyfert 2 galaxy serendipitously observed in the field of NGC 4111.

Subject headings: galaxies: active — galaxies: nuclei — X-rays: galaxies

1. Introduction

LINERs (low-ionization nuclear emission-line regions; Heckman 1980) are found in a significant fraction of bright galaxies (Ho, Filippenko, & Sargent 1997a). The ionizing source of LINERs is still under debate (see Filippenko 1996 for a review), with candidate ionization mechanisms being photoionization by low-luminosity active galactic nuclei (AGNs), photoionization by very hot stars, and collisional ionization by fast shocks. Recent observations have shown that at least some LINERs are low-luminosity AGNs (hereafter LLAGNs); see Ho (1999a and references therein) for a review. According to the extensive spectroscopic survey of Ho et al. (1997b), which includes all bright ($B_T \lesssim 12.5$ mag) galaxies with declinations greater than $0°$, about 20% of LINERs exhibit a broad Hα emission line in their optical spectra. Hard X-ray observations provide a powerful means for searching for evidence of an AGN by detecting a pointlike hard X-ray source at the nucleus. Compact hard X-ray sources have been detected in LINERs that show broad Hα emission (hereafter LINER 1s; Iyomoto et al. 1996, 1998; Ptak et al. 1998; Terashima et al. 1998a; Guainazzi & Antonelli 1999; Weaver et al. 1999). The X-ray spectra of these objects are well represented by a two-component model: a power-law component plus soft thermal emission. The X-ray spectra of the hard component are quite similar to those of Seyfert galaxies, and typical X-ray luminosities are 10^{40-41} ergs s^{-1}. The Hα luminosities of LINER 1s are positively correlated with the X-ray luminosities in the 2–10 keV band (Terashima 1999; Terashima et al. 1999). These observations strongly support the idea that most LINER 1s are LLAGNs.

LINERs constitute the majority of the objects that show spectroscopic evidence for nuclear activity, and most LINERs ($\sim 80\%$; Ho et al. 1997a, b) show no detectable broad Hα emission and are classified as "LINER 2s". Therefore, LINER 2s are the most abundant form of low-level activity in nearby galaxies. It is not clear whether the origin of LINER 2s is similar to that of

LINER 1s. If LINER 2s are also genuine AGNs, then the emission from their nuclei may be obscured, by analogy with the popular obscuration model for Seyfert 2 galaxies (Lawrence & Elvis 1982; Antonucci & Miller 1985). If this is the case, then the X-ray spectra of LINER 2s should show evidence for heavy absorption ($N_H > 10^{23}$ cm^{-2}) and strong fluorescent iron K emission lines. For example, NGC 1052, a LINER 1.9 (Ho et al. 1997a) from which polarized broad Hα line has been detected (Barth et al. 1999), shows an X-ray spectrum absorbed by a column density of $N_H \approx 3 \times 10^{23}$ cm^{-2} and a fluorescent iron K emission line with an equivalent width of $\sim$300 eV (Weaver et al. 1999). These X-ray characteristics are quite similar to those of luminous Seyfert 2 galaxies (Awaki et al. 1991a; Smith & Done 1994; Turner et al. 1997a). Thus, this is an example of an active nucleus which is a low-ionization analog of Seyfert 2 galaxies such as NGC 1068.

Alternatively, the optical emission lines in LINER 2s may be ionized by sources other than an AGN. Collisional ionization from fast-moving shocks (e.g., Koski & Osterbrock 1976; Fosbury et al. 1978; Dopita & Sutherland 1995) and photoionization by a cluster of hot, young stars (Terlevich & Melnick 1985; Filippenko & Terlevich 1992; Shields 1992) have also been proposed as possible excitation mechanisms to power the narrow-line emission in LINERs. Ultraviolet (UV) spectra of several LINER 2s are available from the *Hubble Space Telescope* (*HST*), and these indicate the presence of massive stars in some LINER 2s (Maoz et al. 1998). Maoz et al. (1998) find that in NGC 404, NGC 4569, and NGC 5055 hot stars play a significant role as an ionizing source for the optical emission lines. In order to explain the observed Hα luminosities by stellar photoionization, however, very massive stars ($M \approx 100\ M_\odot$) are required to be still present (see Fig. 5 in Maoz et al. 1998).

Although UV spectroscopy can probe the presence of massive stars, only UV bright objects ($\sim$20%–30% of LINERs; Maoz et al. 1995; Barth et al. 1998; Ho, Filippenko, & Sargent 1999) can be studied. Moreover, Maoz et al. (1998) have argued that even in objects such as M81, NGC 4579 or NGC 4594, where an LLAGN is known to be present based on other evidence, the observed UV continuum power is insufficient to account for the observed line emission, and the nonstellar component most likely becomes more prominent at higher energies. Searching for the ionizing source in the X-rays is necessary to test this hypothesis.

Only a limited number of X-ray observations of LINER 2s have been performed so far. Previous X-ray observations with *Einstein* and *ROSAT* were limited to soft energies, where heavily obscured AGNs are difficult to detect. Furthermore, the limited spectral resolution and bandpass of these observations cannot distinguish the thermal emission of the host galaxy from the emission from the AGN.

We observed a small sample of three LINER 2 nuclei (NGC 404, NGC 4111, and NGC 4457) with the *ASCA* satellite to search for a hidden ionizing source; the sample also included NGC 4192 and NGC 4569, which are classified as "transition objects," emission-line nuclei whose optical spectra suggest a composite source of ionization. possibly due to a genuine LINER nucleus mixed in with signal from circumnuclear H II regions. The imaging capability of *ASCA* (Tanaka,

Inoue, & Holt 1994), which extends up to 10 keV, and its moderate spectral resolution enable it to identify thermal emission from the host galaxy. We also analyze the X-ray properties of NGC 4117, a low-luminosity Seyfert 2 galaxy serendipitously observed in the field of NGC 4111.

This paper is organized as follows. In §2 we summarize the *ASCA* observations and data reduction. Image and spectral analysis are reported in §3 and §4, respectively. We discuss the origin of X-ray emission and the ionizing source in type 2 LINERs in §5. A summary of our findings is presented in §6.

2. Observations

We observed the three LINER 2s and two transition objects shown in Table 1. These objects are selected from the Palomar survey of nearby galaxies conducted by Ho et al. (1995, 1997a), for which Ho et al. (1997b) determined that broad Hα emission is not present. We selected objects that are bright in the narrow Hα emission line, since a large X-ray flux is expected if the ionization source is due to an AGN (Halpern, & Steiner 1983; Elvis, Soltan, & Keel 1984; Ward et al. 1988; Koratkar et al. 1995; Terashima 1999; Terashima et al. 1999). We also gave preference to objects that have previously been studied in the UV using the *HST*. Both NGC 404 and NGC 4569 are UV bright and have been studied spectroscopically in the UV by Maoz et al. (1998), while NGC 4111 and NGC 4192 were imaged in the UV but were not detected (Maoz et al. 1996; Barth et al. 1998).

The log of the *ASCA* observations is shown in Table 2. Detailed descriptions of the *ASCA* instruments can be found in Serlemitsos et al. (1995), Ohashi et al. (1996), Makishima et al. (1996), Burke et al. (1994), and Yamashita et al. (1997). The observation mode of the Solid-state Imaging Spectrometers (SIS) is summarized in Table 2; the Gas Imaging Spectrometers (GIS) were operated in the nominal pulse-height mode. We screened the data using standard criteria. We excluded data taken when (1) the elevation angle from the earth's limb was less than 5° , (2) the cut-off rigidity was less than 6 GeV c^{-1}, (3) the satellite was passing through the South Atlantic Anomaly, and (4) the elevation angle from the day earth's limb was less than 25° (only for the SIS). The observed count rates, after background subtraction, and the net exposure times, after data screening, are also tabulated in Table 2. Although we observed NGC 404, 4111, 4192 and 4569 on two occasions in order to search for variability, no significant variability was found. The typical upper limit on variability is 50%. We therefore use images and spectra combined from the two observations in the following analysis. In this paper, the quoted errors are at the 90% confidence level for one parameter of interest, unless otherwise noted.

3. X-ray images

We detected X-ray emission from all objects except for NGC 404. In this section, we show X-ray images and estimate the spatial extension of the X-ray emission.

3.1. NGC 404

The nucleus of NGC 404 was not detected in either the SIS or in the GIS images. One serendipitous source was detected in the SIS image in the 0.5–2 keV band of the second observation. The SIS image in the 0.5–2 keV band is shown in Figure 1a. The peak position of this source is $(\alpha, \delta)_{\mathrm{J2000}} = (1^h 9^m 28^s, 35° 38' 59'')$, and the error radius is about $1'$. This source is not clearly seen in the GIS image or in the SIS image above 2 keV.

We calculated an upper limit for the X-ray flux seen toward the nucleus of NGC 404 using the following procedure. We made a one-dimensional projection of width $2\rlap{.}'5$ along the nucleus and the serendipitous source and then fitted the profile with a model consisting of two point-spread functions (PSFs) at the positions of the two objects plus a constant background. The model PSFs were obtained using a ray-tracing code, and they were projected using the same method applied to the data. The free parameters are the normalizations of the two PSFs and the background level. We fitted the projected SIS images in the 0.5–2 keV and 2–10 keV bands and obtained a 3σ upper limit of 1.1×10^{-14} ergs s^{-1} cm^{-2} and 6.6×10^{-14} ergs s^{-1} cm^{-2}, respectively, assuming a power-law spectrum with a photon index of $\Gamma = 2$. For an assumed distance of 2.4 Mpc (Tully 1988), these upper limits for the X-ray flux correspond to luminosities of 7.6×10^{36} ergs s^{-1} in the 0.5–2 keV band and 4.6×10^{37} ergs s^{-1} in the 2–10 keV band.

3.2. NGC 4111

Figures 1c and 1d show the GIS images in the 0.5–2 keV and 2–7 keV bands, respectively. At least three X-ray sources were detected in the GIS field of view, and the positions and tentative identifications of these are summarized in Table 3. One of these sources, at $(\alpha, \delta)_{\mathrm{J2000}} = (12^h 7^m 47^s, 43° 6' 53'')$ is brighter in the >2 keV image than in the <2 keV image. This hard source is positionally coincident, within the astrometric uncertainty of *ASCA*, with NGC 4117, a $B \approx 14.0$ mag Seyfert 2 galaxy first recognized by Huchra, Wyatt, & Davis (1982). The other two sources are brighter in the soft-band image. One of the soft sources coincides with the nucleus of NGC 4111, while the other has no counterpart in the NASA Extragalactic Database (NED).

NGC 4111 is detected also in the SIS image, but the other sources are out of the field of view of the detector. In order to estimate the spatial extent of the X-ray emission, we made azimuthally averaged radial profiles of surface brightness using the SIS images and compared them with those of the PSF. We used the SIS images to examine the spatial extent of the emission, since the

spatial resolution of the SIS is better than that of the GIS. We tried to fit the radial profiles in the 0.5–2 keV and 2–7 keV bands with a PSF plus constant background model. The free parameters are the normalization of the PSF and the background level. The fits were unacceptable: $\chi^2 =$ 20.9 and 30.4 for 11 degrees of freedom, in the 0.5–2 keV and 2–7 keV bands, respectively. In order to parameterize the spatial extent. we fitted the radial profiles with a constant background plus a two-dimensional Gaussian convolved through the PSF. The free parameters in this fit are the dispersion and normalization of the Gaussian and the background level. This model gave a significantly better fit with $\Delta\chi^2 = 14$ and 21, respectively, for one additional parameter. These are significant at more than 99% confidence. The best-fit values of σ are summarized in Table 4. The Gaussian model provides a reasonably good representation of the observed profile. These results indicate that the X-ray images are extended on kpc scales in both the 0.5–2 keV and 2–7 keV bands. The difference in spatial extent between the two energy bands is not significant. The best-fit profile is shown in Figure 2.

3.3. NGC 4192

NGC 4192 and a few serendipitous sources were detected in the field. The contour maps of the SIS images in the 0.5–7 keV band are shown in Figure 1*b*. The positions of the detected sources are summarized in Table 3. An archival *ROSAT* PSPC image shows two sources, which combine to yield an elongated morphology, centered on the galaxy. The position angle of the elongation is ~ 72 deg and these sources are aligned roughly along the direction of the minor axis of the galaxy. In the *ASCA* image, this elongation is not clearly seen because of limited photon statistics and spatial resolution.

Since NGC 4192 is very dim and its exposure time was shorter than those of other objects, we fitted the one-dimensional projection of the SIS images. as in the case of NGC 404, to measure the X-ray fluxes; the projection was made with a width of 3′2 along the nucleus and the serendipitous source (source 3 in Table 3). We fitted the resulting profile with a constant background plus two PSFs centered at the position of the galaxy nucleus and source 3. The free parameters in the fit are the normalization of each PSF and the background level. The fit of the projected profiles in the 0.5–2 keV and 2–10 keV bands yielded X-ray fluxes of 5.7×10^{-14} ergs s^{-1} cm^{-2} and 1.1×10^{-13} ergs s^{-1} cm^{-2}, respectively, for an assumed power-law spectrum with $\Gamma = 1.7$ (see § 4). At an adopted distance of 16.8 Mpc (Tully 1988). these fluxes correspond to the luminosities of $L(0.5$–2 keV$) = 1.9 \times 10^{39}$ ergs s^{-1} and $L(2$–10 keV$) = 3.8 \times 10^{39}$ ergs s^{-1}. The significance of the detection is 9.6σ and 6.7σ in the 0.5–2 keV and 2–10 keV bands, respectively.

3.4. NGC 4457

NGC 4457 was detected in both the SIS and GIS images. Contour maps of GIS images in the 0.5–2 keV and 2–7 keV bands are shown in Figure 1e and 1f. Serendipitous sources are also detected in the GIS field of view, and their positions are summarized in Table 3. The brightest one, located at $(\alpha, \delta)_{\mathrm{J2000}} = (12^h 29^m 47^s, 3° 35' 32'')$, is plausibly identified with the Virgo cluster galaxy VCC 1208 $[(\alpha, \delta)_{\mathrm{J2000}} = (12^h 29^m 39.2^s, 3° 36' 43'')]$.

We fitted the radial profiles of the SIS images in the 0.5–2 keV and 2–7 keV bands using the same procedure as in NGC 4111. The PSF fits gave χ^2 values of 26.9 and 15.3, respectively, for 11 degrees of freedom. The results of the Gaussian fits are shown in Table 4. The image in the hard band is consistent with being pointlike, but the upper limit on σ is large ($\sigma < 1.8$ arcmin). Although the lower boundary of the Gaussian σ for the soft-band image fit is greater than zero, this result cannot rule out the possibility that the soft X-ray source is pointlike, since it is possible that Gaussian fits to a point source results in nonzero σ ($\lesssim 0.'2$) (Ptak 1997). The best-fit profile is shown in Figure 2.

3.5. NGC 4569

NGC 4569 was detected in both the SIS and GIS images, and a few serendipitous sources were found in the GIS field of view. The GIS images in the 0.5–2 keV and 2–7 keV bands are shown in Figures 1g and 1h. The position of the brightest source $[(\alpha, \delta)_{\mathrm{J2000}} = (12^h 37^m 34^s, 13° 18' 47'')]$ coincides closely with that of the QSO Q1235+1335 $[(\alpha, \delta)_{\mathrm{J2000}} = (12^h 37^m 33.6^s, 13° 19' 6.''6)$; $z=0.15]$. Diffuse emission from the hot gas in the Virgo cluster is also seen in the soft-band image. NGC 4569 is separated from M87 by 2.1 degrees, and the cluster emission at this angular distance has been detected in a *ROSAT* PSPC image by Böhringer et al. (1994).

We compared the radial profiles of the SIS images in the 0.5–2 keV and 2–7 keV bands with those of the PSF and found that the SIS images are clearly extended in both energy bands. The PSF fits yielded $\chi^2 = 37.2$ and 30.7 for 11 degrees of freedom, respectively. The best-fit σ for the Gaussian model is shown in Table 4, and the profiles are shown in Figure 2. The χ^2 improved significantly in this model for one additional parameter ($\Delta\chi^2 = 22$ and 24 for the 0.5–2 keV and 2–7 keV images, respectively). The profile in the 2–7 keV band is well fitted by a Gaussian with $\sigma = 1.'6$. On the other hand, the residuals of the fit in the 0.5–2 keV band suggest the presence of a compact source at the center in addition to the emission extended over arcminute scales. These two components can be identified with the unresolved emission seen in a *ROSAT* HRI image (Colbert & Mushotzky 1999) and the extended emission detected in a *ROSAT* PSPC image (Junkes & Hensler 1996).

4. X-ray spectra

We fitted the X-ray spectra of NGC 4111, 4117, 4457, and 4569. The spectra were extracted using a circular region centered on the nucleus with a radius of $3'-4'$ which is consistent with the sizes of objects. There were no confusing sources within the extraction radius. Background spectra were extracted from a source-free region in the same field. The spectra from the two SIS detectors (SIS0 and SIS1) were combined, as were those from the two GIS detectors (GIS2 and GIS3). Then we fitted the SIS and GIS spectra simultaneously. The Galactic hydrogen column densities used in the spectral fits are derived from the H I observations by Dickey & Lockman (1990). Since NGC 4192 is too faint for a detailed spectral analysis, we estimated its spectral shape using the hardness ratio, defined to be the photon flux ratio between the 2–10 keV and 0.5–2 keV bands.

4.1. NGC 4111, NGC 4457, and NGC 4569

The X-ray spectra of NGC 4111, NGC 4457 and NGC 4569 cannot be fitted with a single-component model. We tried a power-law model and a thermal bremsstrahlung model. The absorption column density of the matter along the line of sight was treated as a free parameter. We obtained unacceptable fits (Table 5). Since the value of the obtained reduced χ^2 is large (> 2), errors are not shown for spectral parameters in Table 5. A bump is seen around 0.8–0.9 keV in all the spectra, which can be identified with the Fe L line complex. This feature suggests the presence of a thermal plasma with a temperature of ~ 0.7 keV. A Raymond-Smith (hereafter RS; Raymond & Smith 1977) thermal plasma model also failed to give an adequate fit, and significant positive residuals were seen above ~ 1.5 keV. This indicates the presence of a hard component in addition to the soft thermal emission. Accordingly, we fitted the spectra with a two-component model which consists of a soft thermal component and a hard component. We used the RS plasma to represent the soft thermal component and a power-law or thermal bremsstrahlung contribution as the hard component. We assumed a Galactic value for the absorption column density of the RS component. The abundances were fixed at 0.1 of the solar value since it would otherwise not be well constrained from the data; adopting other values (0.3 and 0.5 solar) gave similar results within the errors. The absorption column density for the hard component is treated as free parameter. Table 5 summarizes the results of the fitting. The two-component model reproduces well the observed spectra, and both a power law and a thermal bremsstrahlung model yield similarly good fits. The observed spectra and the best-fit RS plus power-law models are shown in Figure 3, and Table 7 lists the derived X-ray luminosities. The RS plus thermal bremsstrahlung model gives very similar luminosities.

It is worth noting that the temperatures of the thermal bremsstrahlung component in NGC 4111 and NGC 4457 are not well constrained, and only lower limits of the temperature are obtained. Additionally, if the abundance of the RS component were allowed to vary, only NGC 4111 gives a constrained value (0.006–1.0 solar). We could set only a lower limit of the abundance

for NGC 4457 (>0.001 solar) and NGC 4569 (>0.05 solar).

The X-ray fluxes obtained from SIS and GIS are consistent with each other, within the errors, for NGC 4111 and NGC 4457. In the case of NGC 4569, the SIS and GIS fluxes differ at the level of 20%–50%; the SIS gives ∼ 20% smaller flux in the soft band below 2 keV, while its flux in hard band above 2 keV is ∼ 50% larger. This discrepancy is possibly due to the diffuse emission in the NGC 4569 field and to the different background extract regions. In the spectra of NGC 4569, negative residuals are seen around 1.2 keV. This may be also due to imperfect subtraction of surrounding diffuse emission, since the temperature of the Virgo intracluster gas in this region is ∼ 2.5 keV, and both the Fe L line complex and the He-like Mg line are expected around an energy of 1.1–1.3 keV (Böhringer et al. 1994; Matsumoto 1998). Because the SIS and GIS each has a different spatial resolution and field of view, we cannot perfectly match the source-free region used for background subtraction. Therefore, we regard this discrepancy (up to 50%) as a systematic error inherent in the derive X-ray fluxes and luminosities of NGC 4569. The typical errors for the fluxes and luminosities of NGC 4111 and NGC 4457 are ∼25% (this value does not include the calibration uncertainty of ∼10%).

4.2. NGC 4192

Since NGC 4192 is very faint, we estimated its spectral slope using a hardness ratio, $f(2\text{–}10 \text{ keV})/f(0.5\text{–}2 \text{ keV})$. The photon flux in each energy band was calculated from the fits of the projected image described in § 3.3. We obtained a hardness ratio of 0.48 ± 0.09 (1σ errors). If we assume a spectral shape of a power law absorbed by the Galactic hydrogen column density in the direction of this galaxy ($N_{\rm H} = 2.7 \times 10^{20} \text{ cm}^{-2}$), this hardness ratio corresponds to $\Gamma = 1.70^{+0.19}_{-0.16}$ (1σ errors).

4.3. NGC 4117

For completeness, we mention the results of the spectral analysis for NGC 4117, a low-luminosity Seyfert 2 galaxy serendipitously observed in the GIS field of NGC 4111. It is of great interest to compare the spectral properties of LINER 2s with low-luminosity Seyfert 2s. The GIS spectrum of NGC 4117 is shown in Figure 4. It is clear that the soft X-rays are significantly absorbed by a large column density. We fitted the spectrum with an absorbed power-law model. The best-fit parameters are: $\Gamma = 0.92^{+1.16}_{-0.81}$ and $N_{\rm H} = 2.8^{+1.6}_{-1.0} \times 10^{23} \text{ cm}^{-2}$. Since small positive residuals are seen below 2 keV, we also tried to add a power-law component with little absorption. We assumed that the photon indices of both power laws are the same (equivalent to a partially covered power-law model) and that the absorption column for the less absorbed power-law component is equal to the Galactic value ($N_{\rm H} = 1.4 \times 10^{20} \text{ cm}^{-2}$). In this model, χ^2 improved by only $\Delta\chi^2 = -2.5$, and the resulting best-fit model parameters, as summarized in Table 6, are

$\Gamma = 1.11^{+0.97}_{-1.01}$ and $N_H = 3.0^{+0.9}_{-1.1} \times 10^{23}$ cm^{-2}. The X-ray luminosities for this model are shown in Table 7, where we adopt a distance of 17 Mpc (Tully 1988). The intrinsic X-ray luminosity of 1.3×10^{41} ergs s^{-1} is one of the lowest values ever observed for Seyfert 2 galaxies in the hard X-ray band.

We added a narrow Gaussian to the above models to constrain the Fe K fluorescent line. No significant improvement of χ^2 was obtained. The upper limits of the equivalent width are 150 and 125 eV for the single power-law model and the partially covered power-law model, respectively.

The observed X-ray spectrum obscured by large column density ($N_H > 10^{23}$ cm^{-2}) is quite similar to more luminous Seyfert 2 galaxies. The obtained best-fit photon index is flat (0.9–1.1), although the error is large. It is flatter than the canonical value in Seyfert 1 galaxies (e.g. Nandra et al. 1997) and such an apparently flat spectral slope is often observed in Seyfert 2 galaxies (Awaki et al. 1991a; Smith & Done 1996; Turner et al. 1997a). Seyfert 2 galaxies usually show fluorescent Fe K emission line. Although the upper limit on the equivalent width is slightly smaller than that expected from cold matter of $N_H = 3 \times 10^{23}$ cm^{-2} along the line of sight (150–200 eV; Awaki et al. 1991a; Leahy & Creighton 1993; Ghisellini, Haardt, & Matt 1994), it is consistent with Seyfert 2 galaxies within the scatter in the plot of equivalent width versus absorption column density (Fig 1 in Turner et al. 1997b). Therefore, we found no clear difference between luminous Seyfert 2 galaxies and the low luminosity Seyfert 2 NGC 4117.

5. Discussion

5.1. Hard Component

We have detected hard X-ray emission from all the objects except for NGC 404. The hard X-ray (2–7 keV) images of NGC 4111 and NGC 4569 are clearly extended on scales of several kpc, an indication that a nonstellar, active nucleus is not the primary source of the hard X-ray emission. This is also consistent with the lack of time variability.

Other lines of evidence suggest that at least some of these galaxies have experienced recent star formation. The UV spectra of NGC 404 and NGC 4569, for example, show unambiguous stellar absorption lines arising from young, massive stars (Maoz et al. 1998). Starburst galaxies are also a source of hard X-rays, and their X-ray spectra can be modeled as thermal bremsstrahlung emission with a temperature of several keV (e.g., Moran & Lehnert 1997; Ptak et al. 1997; Persic et al. 1998). However, the morphologies of the hard X-ray emission in starburst galaxies tend to be either pointlike or only slightly extended (Tsuru et al. 1997; Cappi et al. 1999), significantly more compact than observed in our sample. It appears, therefore, that hard X-ray emission associated with starburst activity does not significantly contribute to the emission observed in the objects in our sample, although this conclusion remains at the moment tentative because only a small number of starburst galaxies have been studied in the hard X-rays. Note that the extended

hard X-ray emission in the starburst galaxy M83 is interpreted as due to a collection of X-ray binaries in its bulge (Okada, Mitsuda, & Dotani 1997).

In normal spiral galaxies, X-ray emission comes mainly from discrete sources such as low-mass X-ray binaries (Fabbiano 1989; Makishima et al. 1989). The X-ray size of NGC 4111 and NGC 4569 in the hard band is similar to the optical size. The upper limit on the X-ray size of NGC 4457 is also consistent with its optical size. The extended hard-band images of the above objects are consistent with a discrete source origin. Their X-ray spectra, approximated by a thermal bremsstrahlung model with a temperature of several keV, are as expected from a collection of low-mass X-ray binaries (Makishima et al. 1989). The X-ray luminosities of normal spiral galaxies are roughly proportional to the their optical (B band) light (Fabbiano 1989). Table 8 gives the L_X/L_B values for the galaxies in our sample; taking into consideration the scatter in the L_X-L_B relation, these values agree with those seen in normal galaxies. We conclude that the origin of the extended hard X-ray emission in our sample probably arises from a collection of discrete X-ray sources in the host galaxy, and we find no clear evidence for the presence of an AGN.

Note, however, that our data do not rule out the presence of an AGN. If present, the nonstellar X-ray luminosity in the 2–10 keV band must be significantly smaller than few $\times$ 10^{39} ergs s^{-1}. In the case that an AGN core is heavily obscured by a large column density of $N_H > 10^{24}$ cm^{-2}, then we expect only to see X-ray emission scattered by a warm and/or cold reflector. If the scattering fraction is ~3% (Turner et al. 1997b; Awaki, Ueno, & Taniguchi 1999), an upper limit on the intrinsic luminosity is estimated to be ~ 10^{41} ergs s^{-1}. Recent *BeppoSAX* observations have shown that several X-ray weak Seyfert 2s are highly obscured by Compton-thick matter (Maiolino et al. 1998). Such a situation could also occur in LINER 2s. If a heavily obscured AGN is present, a strong Fe K emission line at 6.4 keV is expected with an equivalent width larger than 1 keV (e.g., Terashima et al. 1998b). Unfortunately, this hypothesis cannot be tested with our data because the limited photon statistics do not permit us to set stringent upper limits on the equivalent width of the Fe K line (typical upper limits of the equivalent widths are ~ 2 keV). We will be able to address this issue with future high-energy observations on missions that have larger effective areas, such as *XMM* and *ASTRO-E*, and that have much finer spatial resolution, such as *Chandra*.

Recent work on massive black holes in (nearly) normal galaxies have shown that the mass of the central black hole is about 1/100 to 1/1000 of the mass of the bulge (e.g., Magorrian et al. 1998). Using this black hole mass - bulge mass correlation and our upper limits on X-ray luminosities of AGN, we can estimate upper limits of the Eddington ratio of the accretion onto massive black holes in the galaxies in our sample. We calculated the black hole mass using the relations $M_{BH} = 0.005 M_{bulge}$ and $M_{bulge} = 5 \times 10^9 M_\odot (L_{bulge}/10^9 L_\odot)^{1.2}$ (Richstone et al. 1998 and references therein).

We used the upper limits on the X-ray luminosities in the 2–10 keV band, of 1.5×10^{39} ergs s^{-1} for NGC 404 and 1×10^{41} ergs s^{-1} for the others, and assumed a bolometric correction of a factor of 10 and a scattering fraction of ~ 3%. The bulge luminosities are calculated by using the

data in Table 11 in Ho et al. 1997a. We obtained upper limits on the Eddington ratios in the range of $(1 - 5) \times 10^{-5}$. Thus we found that mass accretion is taking place with very low accretion rate or at very low efficiency if super massive black holes are present in these galaxies, as is in most galaxies.

5.2. Soft Component

In NGC 4111, NGC 4457, and NGC 4569 we detected soft X-ray emission that can be represented by a Raymond-Smith thermal plasma with $kT \approx 0.65$ keV. Extended hot gas with a temperature $kT < 1$ keV is generally observed in starburst galaxies, and it is interpreted as due to gas shock heated by the collective action of supernovae (e.g., Dahlem, Weaver, & Heckman 1998). The X-ray luminosity of the hot gas component is roughly proportional to the far-infrared (FIR) luminosity: $\log L_X/L_{FIR} \approx -4$ (Heckman, Armus, & Milley 1990; David, Forman, & Jones 1992). We calculated the L_X/L_{FIR} ratios for the galaxies in our sample in order to test the starburst origin of the soft thermal component. We use the X-ray luminosities of the RS component corrected for absorption in the 0.5–4 keV band, and L_{FIR} is calculated from the flux $1.26 \times 10^{-14}(2.58S_{60} + S_{100})$ W m^{-2}, where S_{60} and S_{100} are the flux densities at 60 μm and 100 μm, respectively, in units of janskys (Table 1; see Ho et al. 1997a for details). We used observed total luminosities in the 0.5–2 keV band for NGC 404 and NGC 4192, since we cannot separate the thermal component from the total emission. Relations between soft X-ray luminosities and far infrared luminosities are plotted in Figure 5, where Soft X-ray luminosities are only for a Raymond-Smith plasma component except for NGC 404 and NGC 4192. We compiled X-ray luminosities of the soft thermal component in X-ray bright starburst galaxies in *ASCA* archives (for detailed results, see Okada et al. 1996; Ptak et al. 1997; Dahlem, Weaver, & Heckman 1998; Ptak et al. 1999; Della Ceca et al. 1999; Zenzas et al. 1999; Heckman et al. 1999; Moran, Lehnert, & Helfand 1999). We fitted their *ASCA* spectra with a model consisting of a RS plasma plus a thermal bremsstrahlung and measured intrinsic (absorption corrected) X-ray luminosities of the RS component. These points are also shown in Figure 5. The $\log L_X/L_{FIR}$ values (Table 8 and Figure 5) distribute around a value of $\sim$-3.5 – -4, which is consistent, within the scatter, with what is seen in starburst galaxies. With *ASCA* spatial resolution we can only say that the X-ray size is roughly the same as the optical size, consistent with that indicated by higher resolution *ROSAT* data for starburst galaxies.

The radial profile of the soft X-ray image of NGC 4569 indicates the presence of a compact nuclear component in addition to the extended component ($\sigma > 1'$). A comparison between the radial profiles in the soft and hard bands suggests that the compact component has a soft spectrum which could be identified with an unresolved source seen in the *ROSAT* HRI image of Colbert & Mushotzky (1999). A compact but resolved nuclear source is detected in a UV image of NGC 4569 taken with *HST* (Barth et al. 1998), and absorption features in its UV spectrum indicate that the UV source is a cluster of hot stars (Maoz et al. 1998). The X-ray spectra

of O-type stars can be modeled by a thermal plasma with a temperature of $kT \sim 1$ keV (e.g., Corcoran et al. 1994; Kitamoto & Mukai 1996). Since individual O stars have X-ray luminosities of $10^{32} - 10^{33}$ ergs s^{-1} (e.g., Rosner, Golub, & Vaiana 1985), about 10^7 O stars would be required to explain the X-ray source at the nucleus detected in the *ROSAT* HRI image and in the *ASCA* soft-band image. This number, however, is too large compared to the number of O stars needed to explain the observed Hα luminosity and the strength of the UV continuum (<1000; Maoz 1999). Moreover, we can rule out the possibility of such a giant cluster of O stars from dynamical constraints. A cluster of 10^7 O5 stars, each $\sim$40 $M_\odot$, would amount to a total mass of 4×10^8 $M_\odot$. Even under the unreasonable assumption that stars of lower masses are absent, this mass strongly violates the dynamical mass limit of the nucleus, which has been estimated to be $< 10^6 - 10^7$ $M_\odot$ by Keel (1996). Therefore, we conclude that the hot star contribution to the observed soft X-ray luminosity is minor. This argument also applies to all the objects in our sample, except for NGC 404, for which only an upper limit of X-ray luminosity is available.

Finally, we note that scattered light from a hidden AGN is unlikely to be the source of the soft X-ray emission. If AGN emission is blocked by a large column density along the line of sight, only emission scattered by cold and/or warm material would be observed. If we fit the X-ray spectra below 2 keV with a simple power-law model, the photon indices become steeper than 3 for NGC 4111, NGC 4457, and NGC 4569. This spectral slope is significantly steeper than normally seen in Seyfert 2s, where scattering by warm material is thought to prevail. Cold reflection produces an X-ray spectrum that is flatter than the intrinsic spectrum. Additionally, the extended morphologies of the soft X-ray emission makes it unlikely that the photoionized medium can be maintained at a highly ionized state. Thus the soft component probably does not originate from scattered AGN emission. Instead, the most likely origin for the soft thermal component is supernovae-heated hot gas.

5.3. Ionization Photon Budget

We have found no clear evidence for the presence of an AGN in the galaxies in our sample. In order to compare the ionization source in LINER 2s and transition objects with those of LINER 1s and low-luminosity Seyfert galaxies, we calculated L_X(2–10 keV)$/L_{H\alpha}$ ratios (Table 8), where we used the luminosities of the narrow component of the Hα emission. The $L_X/L_{H\alpha}$ values of the galaxies in our sample are systematically lower, by more than one order of magnitude, compared to LINER 1s and low-luminosity Seyferts (Terashima 1999; Terashima et al. 1999), objects where LLAGNs are almost certainly present. The mean log $L_X/L_{H\alpha}$ is 1.6 for LLAGNs, while the log $L_X/L_{H\alpha}$ values for our sample are smaller than 0.61.

We estimate the number of ionizing photons needed to account for the observed Hα luminosities, assuming a spectral energy distribution of $f_\nu \propto \nu^{-1}$, which is the typical spectral shape between the UV and X-rays observed in LLAGNs (Ho 1999b), Case B recombination (Osterbrock 1989), and a covering factor of unity for the ionized gas. A value of log $L_X/L_{H\alpha}$

$= 1.4$ is sufficient to explain the Hα luminosity by photoionization by an AGN. The observed log $L_X/L_{H\alpha}$ values, on the other hand. are significantly lower than this. If the AGN is not significantly obscured, its luminosity in the 2–10 keV band is estimated to be less than a few $\times$ 10^{39} ergs s^{-1}. In this case. photons from an AGN account for only a very small fraction ($\sim 5\%$) of the observed Hα luminosity. If Hα is due to ionization by an AGN. one would then have to postulate that the AGN is heavily obscured with a column density greater than $\sim 10^{24}$ cm^{-2} and that only scattered radiation is observable. Alternatively, an ionizing source other than an AGN is required.

As discussed in the next subsection, galaxies in our sample have lower [OI]λ6300/Hα values than LINERs that are most likely to be AGN. If the low [O I]/Hα ratio is due to dilution by H II regions, which produce strong Balmer lines and very weak [OI], the difference in $L_X/L_{H\alpha}$ between the two classes is reduced. Since the median of the [OI]/Hα ratio for the LINER 2s is about a factor of 3 smaller than that for the LINER 1s with LLAGNs, the Hα emission tracing the AGN would be 1/3 of the total measured value. Even in this case, however, the observed hard X-ray luminosities are not enough to drive the Hα luminosities.

5.4. Optical Emission Line Ratios and Ionizing Source

Our sample includes three LINERs (NGC 404, NGC 4111, and NGC 4457) and two transition objects (NGC 4192 and NGC 4569). By the definition of Ho et al. (1993, 1997a), transition objects have a smaller [O I] λ6300/Hα ratio than LINERs (Table 8; data from Ho et al. 1997a). This class of emission-line nuclei has been postulated to be composite systems where a LINER nucleus is spatially contaminated by circumnuclear star-forming regions (Ho et al. 1993; Ho 1996). On the other hand, photoionization by hot stars in environments with ionization parameters characteristically lower than in "normal" giant extragalactic H II regions also generates the spectral properties of transition objects (Filippenko, & Terlevich 1992; Shields 1992). The presence of hot stars is seen directly in the UV spectrum of NGC 4569 (Maoz et al. 1998); these stars can provide the power to explain the observed emission-line luminosities if very massive stars are still present. The low X-ray output of these systems, as found in this study. lends further support for this conclusion. Thus, at least some transition objects are likely to be powered by hot stars. The nucleus of NGC 4192. however, is not detected in the UV band, possibly because of the large extinction due to the high inclination of the galaxy (83°; Barth et al. 1998). The X-ray properties and optical emission-line ratios of NGC 4192 are similar to those of NGC 4569, and it, too. might be primarily powered by hot stars.

We compared the [O I]/Hα ratios of the LINERs in our sample with those of LINERs from which AGN-like X-ray emission has been detected. The [O I]/Hα ratios for NGC 404. NGC 4111. and NGC 4457 (Table 8) are lower than in LINERs that are strong LLAGN candidates. and they are located at the lowest end of the distribution of [O I]/Hα in LINERs (Fig. 7 in Ho et al. 1997a). For comparison, the [O I]/Hα values for the few LINERs where compact hard X-ray emission

has been detected are 0.71 (NGC 1052), 0.53 (NGC 3998), 1.22 (NGC 4203), 0.48 (NGC 4579), 0.18 (NGC 4594), and 0.24 (NGC 4736).[3] It is intriguing that the *HST* UV spectrum of NGC 404 also shows strong evidence for the presence of energetically significant hot stars (Maoz et al. 1998); no UV spectral information is available for NGC 4111 and NGC 4457. It is conceivable that the subset of LINERs with exceptionally weak [O I] emission owe their primary excitation mechanism to stellar photoionization. Obviously more observations are necessary to settle this issue. A statistical study using a large sample of objects will be presented elsewhere.

6. Summary

We presented *ASCA* results for a small sample of LINERs (NGC 404, NGC 4111, and NGC 4457) and transition objects (NGC 4192 and NGC 4569). X-ray emission was detected in all objects except NGC 404. The X-ray luminosities in the 2–10 keV band range from 4×10^{39} to 1×10^{40} ergs s^{-1}. The images of NGC 4111 and NGC 4569 are extended on scales of several kpc in both the soft (<2 keV) and hard (>2 keV) energy bands. The X-ray spectra of NGC 4111, NGC 4457, and NGC 4569 are well represented by a two-component model consisting of a soft thermal plasma of $kT \sim 0.65$ keV plus a hard component (power law or thermal bremsstrahlung).

The soft X-ray emission probably originates from hot gas produced via recent star formation activity because both the temperature of the gas and the L_X/L_{FIR} ratios are typical of starburst galaxies. The extended morphology of the hard X-ray emission indicates that it mainly comes from discrete sources in the host galaxies, and that the AGN contribution is small, if any. The L_X(2–10 keV)/$L_{H\alpha}$ values for the galaxies in our sample are more than one order of magnitude smaller than in LINERs with bona fide LLAGNs (those with a detectable broad Hα emission line and compact hard X-ray emission), and the X-ray luminosities are insufficient for driving the optical emission-line luminosities. These facts imply that, if an AGN is present, it would have to be heavily obscured with a column density much greater than $N_H \approx 10^{23}$ cm^{-2}. We suggest that the optical emission lines in the galaxies in our sample are mainly powered by photoionization by hot, young stars rather than by an AGN. This hypothesis is supported by the detection of stellar features due to massive stars in the UV spectra of NGC 404 and NGC 4569, by the systematically lower [O I]/Hα ratios in these objects compared to LINERs with bona fide LLAGNs, and by the low observed X-ray luminosities reported in this work.

We also analyzed the X-ray properties of NGC 4117, a low-luminosity Seyfert 2 galaxy serendipitously observed in the field of NGC 4111, and found its properties to be consistent with other Seyfert 2 galaxies with moderate absorbing columns.

---

[3]The X-ray results for these objects are published in Weaver et al. (1999), Guainazzi, & Antonelli (1999), Awaki et al. (1991b), Iyomoto et al. (1998), Terashima et al. (1998a), Nicholson et al. (1998), and Roberts et al. (1999).

REFERENCES

Antonucci, R. R. J., & Miller, J. S. 1985, ApJ, 297, 621

Awaki, H., Koyama, K., Inoue, H., & Halpern, J. P. 1991a, PASJ, 43, 195

Awaki, H., Koyama, K., Kunieda, H., Takano, S., Tawara, Y., & Ohashi, T. 1991b, ApJ, 366, 88

Awaki, H., Ueno, S., & Taniguchi, Y. 1999, in The 32nd COSPAR Meeting, Broad band X-ray Spectra of Cosmic Sources, ed. K. Makishima, & L. Piro (Advances in Space Research), in press

Barth, A. J., Filippenko, A. V., & Moran, E. C. 1999, ApJ, 515, L61

Barth, A. J., Ho, L. C., Filippenko, A. V., & Sargent, W. L. W. 1998, ApJ, 496, 133

Barth, A. J., Reichert, G. A., Filippenko, A. V., Ho, L. C., Shields, J. C., Mushotzky, R. F., & Puchnarewicz, E. M. 1996, AJ, 112, 1829

Barth, A. J., Reichert, G. A., Ho, L. C., Shields, J. C., Filippenko, A. V., & Puchnarewicz, E. M. 1997, AJ, 114, 2313

Böhringer, H., Briel, U. G., Schwarz, R. A., Voges, W., Hartner, G., & Trümper, T. 1994, Nature, 368, 828

Burke, B. E., Mountain, R. W., Daniels, P. J., & Dolat, V. S. 1994, IEEE Trans. NS-41, 375

Cappi, M., et al. 1999, in The 32nd COSPAR Meeting, The AGN-Galaxy Connection, ed. H. R. Schmitt, A. L. Kinney, & L. C. Ho (Advances in Space Research), 23, 905

Colbert, E. J. M., & Mushotzky, R. F. 1999, ApJ, 519, 89

Corcoran, M. F., et al. 1994, ApJ, 436, L95

Dahlem, M., Weaver, K. A., & Heckman, T. M. 1998, ApJS, 118, 401

Della Ceca, R., Griffiths, R. E., Heckman, T. M., Lehnert, M. D., & Weaver, K. A. 1999, ApJ, 514, 772

Dickey, J. M., & Lockman, F. J. 1990, ARA&A, 28, 215

Dopita, M. A., & Sutherland, R. S. 1995, ApJ, 455, 468

Elvis, M., Soltan, A. & Keel, W. C. 1984, ApJ, 283, 479

Fabbiano, G. 1989, ARA&A, 27, 87

Filippenko, A. V. 1996, in The Physics of LINERs in View of Recent Observations, ed. M. Eracleous et al. (San Francisco: ASP), 17

Filippenko, A. V., & Terlevich, R. 1992, ApJ, 397, L79

Fosbury, R. A. E., Melbold, U., Goss, W. M., & Dopita, M. A. 1978, MNRAS, 183, 549

Ghisellini, G., Haardt, F., & Matt, G. 1994, MNRAS, 267, 743

Guainazzi, M. & Antonelli, L. A. 1999, MNRAS, 304, L15

Halpern, J. P., & Steiner, J. E. 1983, ApJ, 269, L37

Heckman, T. M. 1980, A&A, 87, 152

Heckman, T. M., Armus, L., & Miley, G. K. 1990, ApJS, 74, 833

Heckman, T. M., Armus, L., Weaver, K. A., & Wang, J. 1999, ApJ, 517, 130

Ho, L. C. 1996, in The Physics of LINERs in View of Recent Observations, ed. M. Eracleous et al. (San Francisco: ASP), 103

Ho, L. C. 1999a, in The 32nd COSPAR Meeting, The AGN-Galaxy Connection, ed. H. R. Schmitt, A. L. Kinney, & L. C. Ho (Advances in Space Research), 23, 813

Ho, L. C. 1999b ApJ, 516, 672

Ho, L. C., Filippenko, A. V., & Sargent, W. L. W. 1993, ApJ, 417, 63

Ho, L. C., Filippenko, A. V., & Sargent, W. L. W. 1995, ApJS, 98, 477

Ho, L. C., Filippenko, A. V., & Sargent, W. L. W. 1996, ApJ, 462, 183

Ho, L. C., Filippenko, A. V., & Sargent, W. L. W. 1997a, ApJS, 112, 315

Ho, L. C., Filippenko, A. V., & Sargent, W. L. W. 1999, in preparation

Ho, L. C., Filippenko, A. V., Sargent, W. L. W., & Peng, C. Y. 1997b, ApJS, 112, 391

Huchra, J. P., Wyatt, W. F., & Davis, M. 1982, AJ, 87, 1628

Iyomoto, N., Makishima, K., Fukazawa, Y., Tashiro, M., Ishisaki, Y., Nakai, N., & Taniguchi, Y. 1996, PASJ, 48, 231

Iyomoto, N., Makishima, K., Matsushita, K., Fukazawa, Y., Tashiro, M.. & Ohashi, T. 1998, ApJ, 503, 168

Keel, W. C. 1983, ApJS, 52, 229

Keel, W. C. 1996, PASP, 108, 917

Koski, A. T., & Osterbrock, D. E. 1976, ApJ, 203, L49

Junkes, N., & Hensler, G. 1996, MPE report 263, 459

Kitamoto, S. & Mukai, K. 1996, PASJ, 48, 813

Koratkar, A. P., Deustua, S. E., Heckman, T. M., Filippenko, A. V., Ho, L. C., & Rao, M. 1995, ApJ, 440, 132

Lawrence, A., & Elvis, M. 1982, ApJ, 256, 410

Leahy, D., & Creighton, J. 1993, MNRAS, 263, 314

Magorrian, J. et al. 1998, AJ, 115, 2285

Maiolino, R., et al. 1998, A&A, 338, 781

Makishima, K., et al. 1989, PASJ, 41, 697

Makishima, K., et al. 1996, PASJ, 48, 171

Maoz, D., Filippenko, A. V., Ho, L. C., Macchetto, F. D., Rix, H.-W., & Schneider, D. P. 1996, ApJS, 107, 215

Maoz, D., Filippenko, A. V., Ho, L. C., Rix, H-W., Bahcall, J. N., Schneider, D. P., & Macchetto, F. D. 1995, ApJ, 440, 91

Maoz, D., Koratkar, A. P., Shields, J. C., Ho, L. C., & Filippenko, A. V. 1998, AJ, 116, 55

Maoz, D. 1999, in The 32nd COSPAR Meeting, The AGN-Galaxy Connection, ed. H. R. Schmitt, A. L. Kinney, & L. C. Ho (Advances in Space Research), 23, 855

Matsumoto, H. 1998, Ph.D. thesis, Kyoto University

Moran, E. C., Lehnert, M. D., & Helfand, D. J. 1999, ApJ, in press (astro-ph/9907036)

Nandra K., George I. M., Mushotzky R. F., Turner T. J., Yaqoob T 1997, ApJ 477, 602

Nicholson, K. L., Reichert, G. A., Mason, K. O., Puchnarewicz, E. W., Ho, L. C., Shields, J. C., & Filippenko, A. V. 1998, MNRAS, 300, 893

Ohashi, T., et al. 1996, PASJ, 48, 157

Okada, K., Mitsuda, K., & Dotani, T. 1997, PASJ, 49, 653

Osterbrock, D. E. 1989, Astrophysics of Gaseous Nebulae and Active Galactic Nuclei (Mill Valley: Univ. Science Books)

Ptak, A., Serlemitsos, P., Yaqoob, T., Mushotzky, R., & Tsuru, T. 1997, AJ, 113, 1286

Ptak, A., Serlemitsos, P. J., Yaqoob, T., & Mushotzky, R. F. 1999, ApJS, 120, 179

Ptak, A., Mushotzky, R. F., Yaqoob, T., & Serlemitsos, P. J. 1999, ApJ, submitted

Raymond, J. C. & Smith, B. W. 1977, ApJS, 35, 419

Richstone, D. et al. 1998, Nature, 395, A14

Roberts, T. P., Warwick, R. S., & Ohashi, T. 1999, MNRAS, 304, 52

Rosner, R., Golub, L., & Vaiana, G. S. 1985, ARA&A, 23, 413

Serlemitsos, P. J., et al. 1995, PASJ, 47, 105

Shields, J. C. 1992, ApJ, 399, L27

Smith, D. A., & Done, C. 1996, MNRAS, 280, 355

Tanaka, Y., Inoue, H., & Holt, S. S. 1994, PASJ, 46, L137

Terashima, Y., Kunieda, H., Misaki, K., Mushotzky, R. F., Ptak, A. F., & Reichert, G. A. 1998a, ApJ, 503, 212

Terashima, Y., Ptak, A. F., Fujimoto, R., Itoh, M., Kunieda, H., Makishima, K., & Serlemitsos, P. J. 1998b, ApJ, 496, 210

Terashima, Y. 1999, in Proceedings of 3rd INTEGRAL Workshop: The Extreme Universe (Astrophysical Letters & Communications), in press (astro-ph/9905218)

Terashima, Y., et al. 1999, in preparation

Terlevich, R., & Melnick, J. 1985, MNRAS, 213, 841

Tsuru, T. G., Awaki, H., Koyama, K., & Ptak, A. 1997, PASJ, 49, 649

Tully, R. B. 1988, Nearby Galaxies Catalog (Cambridge: Cambridge Univ. Press)

Turner, T. J., George, I. M., Nandra, K., & Mushotzky, R. F. 1997a, ApJS, 113, 23

Turner, T. J., George, I. M., Nandra, K., & Mushotzky, R. F. 1997b, ApJ, 488, 164

Ward, M. J., Done, C., Fabian, A. C., Tennant, A. F., & Shafer, R. A. 1988, ApJ, 324, 767

Weaver, K. A., Wilson, A. S., Henkel, C., & Braatz, J. A. 1999, ApJ, 520, 130

Yamashita, A., et al. 1997, IEEE Trans. NS-44, 847

Zezas, A. L., Georgantpoulos, I., & Ward, M. J. 1998, MNRAS, 301, 915

Table 1: Observed galaxies

Name	Distance[a] [Mpc]	Classification	$\log F(\mathrm{H}\alpha)$ [ergs s^{-1} cm^{-2}]	$\log L(\mathrm{H}\alpha)$ [ergs s^{-1}]	$\log L_{FIR}$ [ergs s^{-1}]	$\log L_B$ [$L_\odot$]
NGC 404	2.4	L2	−13.21	37.63	40.94	8.58
NGC 4111	17.0	L2	−13.14	39.40	—	10.01
NGC 4192	16.8	T2	−13.56	38.97	43.25	10.64
NGC 4457	17.4	L2	−12.99	39.57	42.98	10.05
NGC 4569	16.8	T2	−12.36[b]	40.174[b]	43.34	10.73

Note. — a: Tully (1988); b: Keel (1983); Other data are taken from Ho et al. 1997a.

Table 2: Observation log

Name	Date	SIS mode	SIS count rate [counts s^{-1}]	SIS exposure [ksec]	GIS count rate [counts s^{-1}]	GIS exposure [ksec]
NGC 404	1997 Jul 21	1CCD Faint	—	12.3	—	13.4
	1998 Feb 6	1CCD Faint	—	27.2	—	29.7
NGC 4111	1997 Dec 7	1CCD Faint LD0.48keV[a]	0.008	14.4	0.004	15.6
	1997 Dec 15	1CCD Faint LD0.48keV[a]	0.008	19.0	0.003	21.2
NGC 4192	1997 Dec 17	2CCD Faint/Bright	—	3.9	—	4.3
	1997 Dec 23	2CCD Faint/Bright	—	13.3	—	14.3
NGC 4457	1998 Jun 14–15	1CCD Faint	0.01	42.1	0.005	44.0
NGC 4569	1997 Jun 24–25	1CCD Faint	0.03	21.9	0.006	21.0
	1997 Jul 6-7	1CCD Faint	0.03	19.0	0.007	20.4

Note. — a: Level discriminator is enabled.

Table 3: Positions of serendipitous sources

source No.	position (J2000)	ID
NGC 404		
1*	1h 9m 28s, 35d 38m 52s	
NGC 4111		
0*	12h 7m 6s, 43d 3m 16s	NGC 4111 12h07m03.2s +43d03m55.3s
1	12h 7m 47s, 43d 6m 53s	NGC 4117 12h07m46.1s +43d07m35.0s
2	12h 8m 16s, 43d 3m 12s	
NGC 4192		
0*	12h 13m 49s, 14d 53m 47s	NGC 4192 12h13m48.3s +14d54m01s
1	12h 13m 5s, 14d 54m 57s	
2	12h 13m 9s, 14d 51m 8s	LBQS 1210+1507 12h13m08.0s +14d51m06s
3	12h 14m 12s, 14d 47m 31s	
NGC 4457		
0*	12h 28m 56s, 3d 34m 15s	NGC 4457 12h28m59.2s +03d34m16.1s
1	12h 28m 17s, 3d 38m 43s	
2	12h 28m 28s, 3d 25m 43s	
3	12h 29m 2s, 3d 38m 14s	
4	12h 29m 47s, 3d 35m 32s	VCC 1208 12h29m39.2s +03d36m43s
NGC 4569		
0*	12h36m50s, +13d10m01s	NGC 4569 (12h36m49.8s, +13d09m46s)
1	12h36m30s, +13d07m59s	
2	12h36m34s, +12d58m54s	
3	12h37m34s, +13d18m47s	QSO Q1235+1335 (12h37m33.6s, +13d19m6.6s)

Note. — *: position determined using SIS images. Typical error radius is 1 arcmin.

Table 4: Gaussian fit to radial profiles

Name	Scale	0.5–2 keV		2–7 keV	
		σ	χ^2/dof	σ	χ^2/dof
	[kpc/arcmin]	[arcmin]		[arcmin]	
NGC 4111	4.95	0.50(0.27-0.89)	6.6	1.2(0.37-3.3)	9.2
NGC 4457	5.06	0.43(0.15-0.65)	18.2	0.11(0-1.8)	15.3
NGC 4569	4.89	1.4(1.0-1.8)	15.7	1.6(1.0-3.5)	6.54

Note. — The quoted errors in parentheses are at the 90% confidence level for one interesting parameter. The degree of freedom in the fit is 10.

Table 5: Results of spectral fits

Name	Model	N_{H1}[a] $[10^{22}\mathrm{cm}^{-2}]$	kT[b] [keV]	abundance[c] [solar]	N_{H2}[d] $[10^{22}\mathrm{cm}^{-2}]$	photon index[e] or kT [keV]	χ^2/dof
NGC 4111	Brems				0	0.65	74.3/24
	PL				0	3.1	48.7/24
	RS+Brems	0.014(f)	$0.65^{+0.12}_{-0.14}$	0.1(f)	$0.49^{+2.3}_{-0.49}$	> 5.0	14.9/22
	RS+PL	0.014(f)	$0.65^{+0.12}_{-0.14}$	0.1(f)	$0^{+3.0}$	$0.9^{+1.1}_{-0.6}$	14.4/22
NGC 4457	Brems				0	3.1	70.7/27
	PL				0	2.3	50.1/27
	RS+Brems	0.018(f)	$0.68^{+0.12}_{-0.16}$	0.1(f)	$0.84^{+2.2}_{-0.84}$	> 2.8	17.9/25
	RS+PL	0.018(f)	$0.68^{+0.12}_{-0.16}$	0.1(f)	$1.1^{+2.7}_{-1.1}$	$1.7^{+1.2}_{-0.8}$	18.0/25
NGC 4569	Brems				0	3.9	114.0/35
	PL				0	2.0	98.0/35
	RS+Brems	0.029(f)	$0.67^{+0.09}_{-0.14}$	0.1(f)	$1.2^{+0.8}_{-0.9}$	$5.4^{+25}_{-2.5}$	56.2/32
	RS+PL	0.029(f)	$0.67^{+0.09}_{-0.10}$	0.1(f)	$1.7^{+1.0}_{-1.1}$	2.2 ± 0.7	55.0/32

Note. — The quoted errors in parentheses are at the 90% confidence level for one interesting parameter. (f) denotes a frozen parameter. The model components are as follows: PL = power-law with absorption; Brems = thermal bremsstrahlung with absorption; RS = Raymond-Smith thermal plasma with the Galactic absorption. [a]: Galactic foreground absorption column density, [b]: temperature of the Raymond-Smith component, [c]: abundance of the Raymond-Smith component, [d]: absorption column density of the hard component [e]: photon index of the power-law component or temperature of the thermal Bremsstrahlung component.

Table 6: Spectral fitting results of NGC 4117

Model	N_H $[10^{22}\mathrm{cm}^{-2}]$	Photon index	covering fraction	χ^2/dof
Power-law	28^{+16}_{-10}	$0.92^{+1.16}_{-0.81}$		21.9/17
Partially covered power-law	$0.014^{a}, 30^{+9b}_{-11}$	$1.11^{+0.97}_{-1.01}$	$0.984^{+0.016}_{-0.038}$	19.4/15

Note. — (f) denotes a frozen parameter. [a]: absorption column density of the uncovered (less absorbed) component dominating the lower energy range, [b]: absorption column density of the covered component.
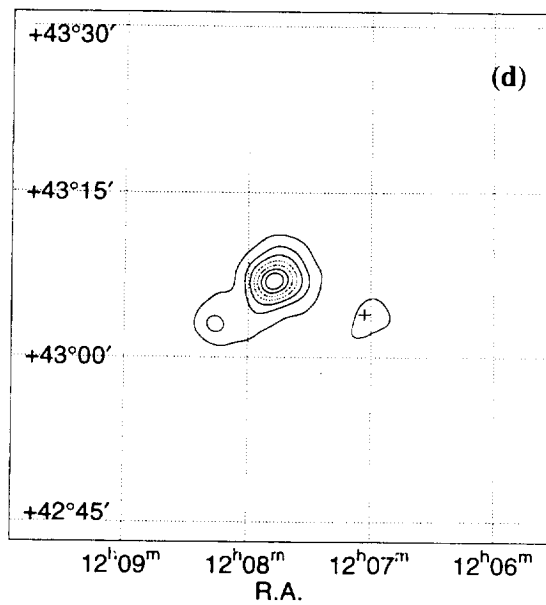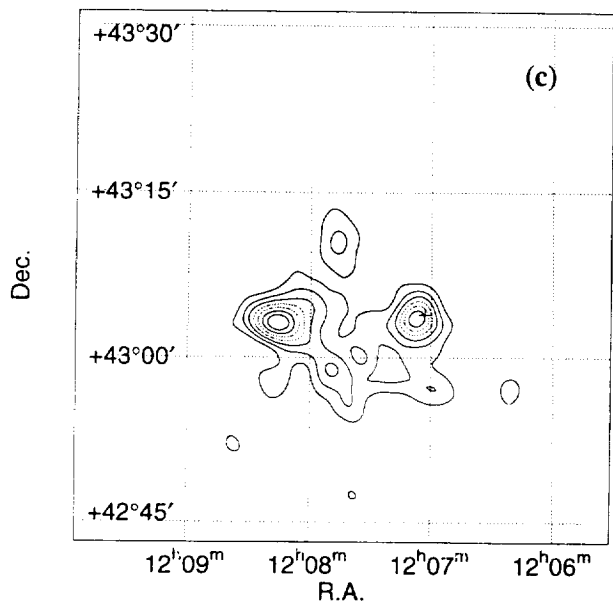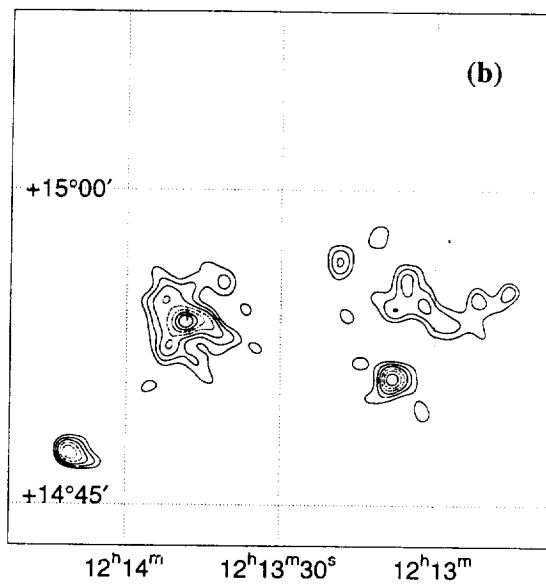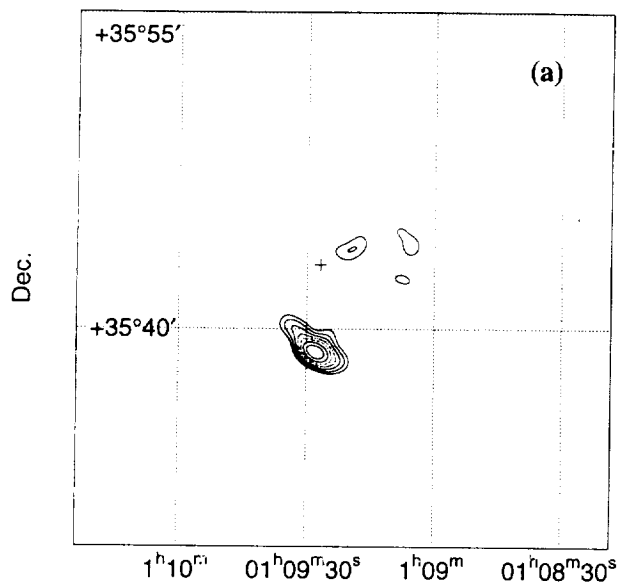
Table 7: X-ray luminosities

Name	Total (2–10 keV) observed	(0.5–2 keV) observed	Power-law (2–10 keV) observed	intrinsic	Raymond-Smith (0.5–4 keV) observed	intrinsic
NGC 404	< 0.046	< 0.0076	—	—	—	—
NGC 4111	9.0	7.1	8.7	8.7	6.0	6.3
NGC 4192	3.8	1.9	—	—	—	—
NGC 4457	9.1	6.4	8.8	9.6	5.6	5.9
NGC 4569	10	8.9	9.8	12	8.0	8.9
NGC 4117	46	0.44	46	130	—	—

Note. — unit: 10^{39} ergs s^{-1}. A RS+PL model is assumed for NGC 4111, 4457, and 4569. The luminosities for NGC 404 and NGC 4192 are obtained from the projected image fitting. A partially covered power-law model is assumed for NGC 4117. Upper limits for NGC 404 are 3σ.

Table 8: Luminosity ratios

	$\log L_{HX}/L_{H\alpha}$	$\log L_{HX}/L_B$	$\log L_{SX}/L_{FIR}$	[O I]/Hα
NGC 404	< 0.03	< −4.52	< −4.06	0.17
NGC 4111	0.54	−3.66	—	0.19
NGC 4192	0.61	−4.65	−3.67	0.14
NGC 4457	0.41	−3.66	−3.21	0.19
NGC 4569	−0.11	−4.26	−3.39	0.062

Note. — L_{HX}: Intrinsic luminosity of the power-law component in 2–10 keV; L_{SX}: Intrinsic luminosity of the Raymond-Smith component in 0.5–4 keV for NGC 4457 and NGC 4569, and observed luminosity in 0.5–2 keV for NGC 404 and NGC 4192
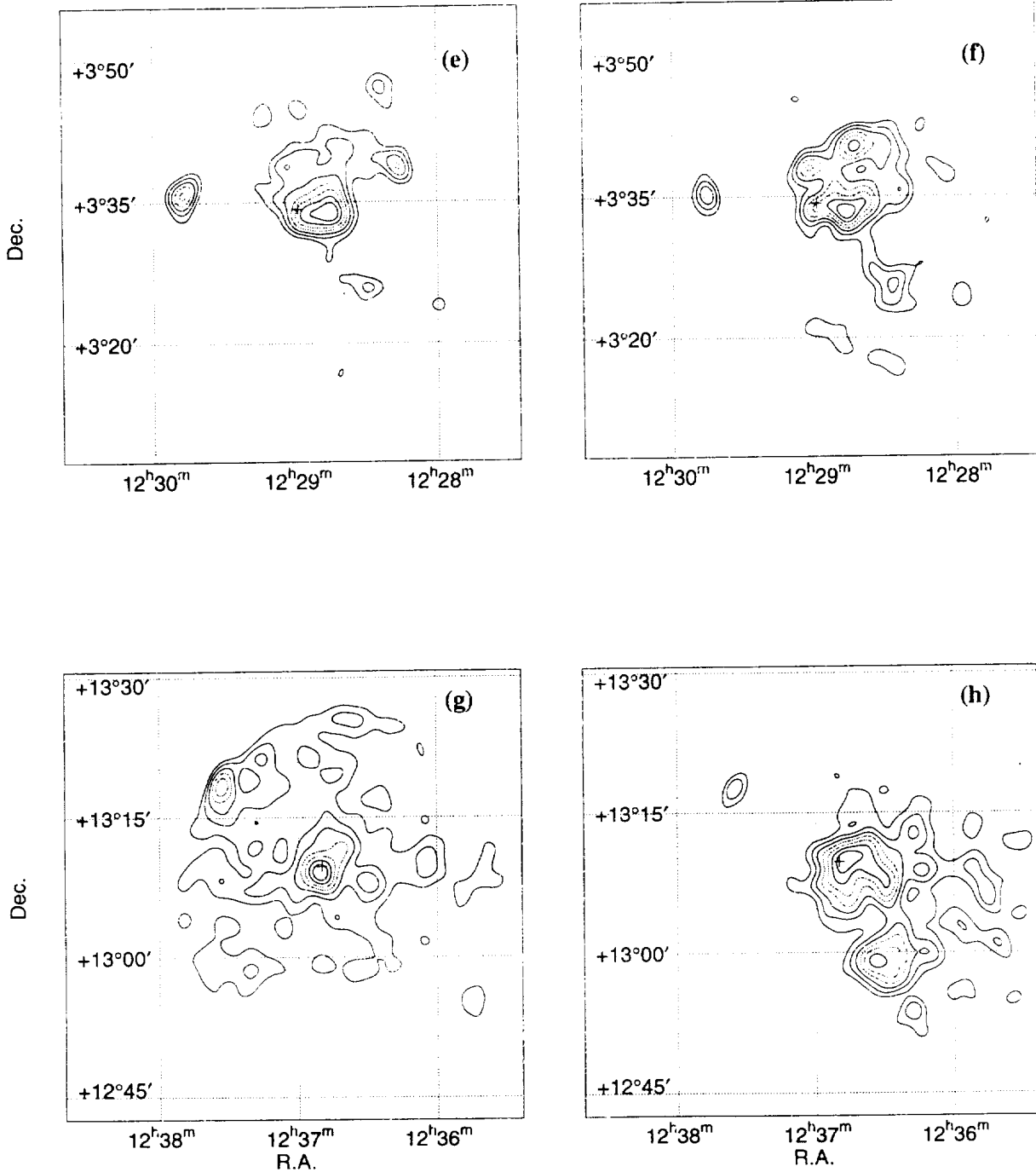
(a)

+35°55′

Dec.

+35°40′

1ʰ10ᵐ   01ʰ09ᵐ30ˢ   1ʰ09ᵐ   01ʰ08ᵐ30ˢ

(b)

+15°00′

+14°45′

12ʰ14ᵐ   12ʰ13ᵐ30ˢ   12ʰ13ᵐ

(c)

+43°30′

+43°15′

Dec.

+43°00′

+42°45′

12ʰ09ᵐ   12ʰ08ᵐ   12ʰ07ᵐ   12ʰ06ᵐ

R.A.

(d)

+43°30′

+43°15′

+43°00′

+42°45′

12ʰ09ᵐ   12ʰ08ᵐ   12ʰ07ᵐ   12ʰ06ᵐ

R.A.

Fig. 1.— (*a*) SIS image of NGC 404 from 0.5–2 keV, (*b*) SIS image of NGC 4192 from 0.5–7 keV. (*c*) GIS image of NGC 4111 from 0.7–2 keV, (*d*) GIS image of NGC 4111 from 2–10 keV. (*e*) GIS image of NGC 4457 from 0.7–2 keV, (*f*) GIS image of NGC 4457 from 2–7 keV, (*g*) GIS image of NGC 4569 from 0.7–2 keV, (*h*) GIS image of NGC 4569 from 2–7 keV. The crosses indicate the optical position of the nucleus taken from the NED. The contours are linearly spaced. The lowest contour levels are (a)40%, (b) 40%, (c) 25%, (d) 15%, (e) 40%, (f) 45%, (g) 40%, and (h) 45% of the peak. Background is not subtracted in these images. Sky coordinates are J2000.
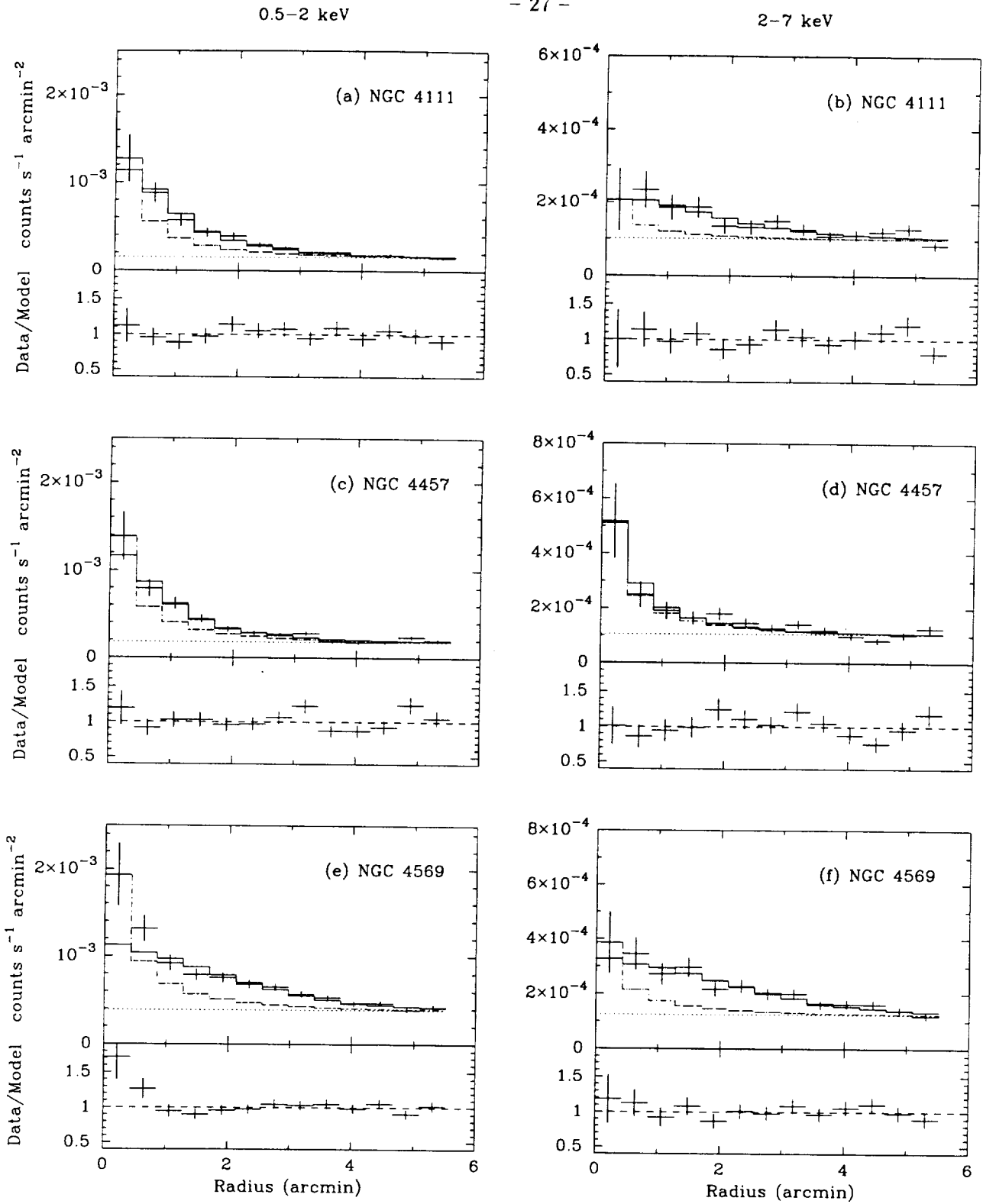
0.5–2 keV

2–7 keV

Fig. 2.— Radial surface brightness profiles fitted with a two- dimensional Gaussian convolved through the PSF + constant model. *Solid* lines are the best-fit model and *dotted* lines are the background level. *Dot-dashed* lines are the PSF normalized at the innermost data point. (*a*) NGC 4111, 0.5–2 keV, (*b*) NGC 4111, 2–7 keV, (*c*) NGC 4457, 0.5–2 keV, (*d*) NGC 4457, 2–7 keV, (*e*) NGC 4569, 0.5–2 keV, (*f*) NGC 4569, 2–7 keV.
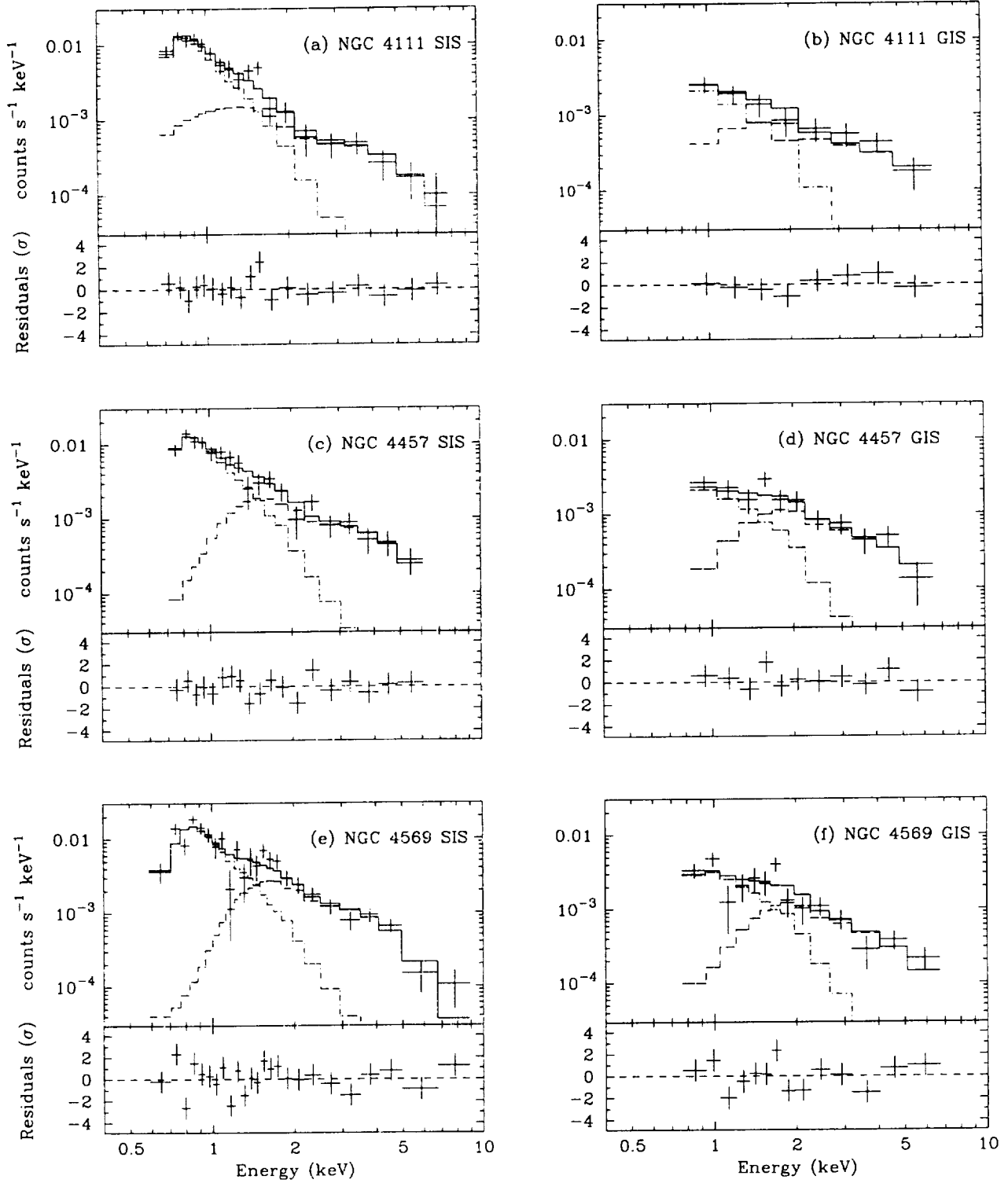
Fig. 3.— (*a*) SIS spectrum of NGC 4111, (*b*) GIS spectrum of NGC 4111, (*c*) SIS spectrum of NGC 4457, (*d*) GIS spectrum of NGC 4457, (*e*) SIS spectrum of NGC 4569, (*f*) GIS spectrum of NGC 4569. Crosses are the observed data and histograms are the best-fit Raymond-Smith + absorbed power-law model. The Raymond-Smith component is plotted with a *dot-dashed* line, and the power-law component is plotted with a *dashed* line.
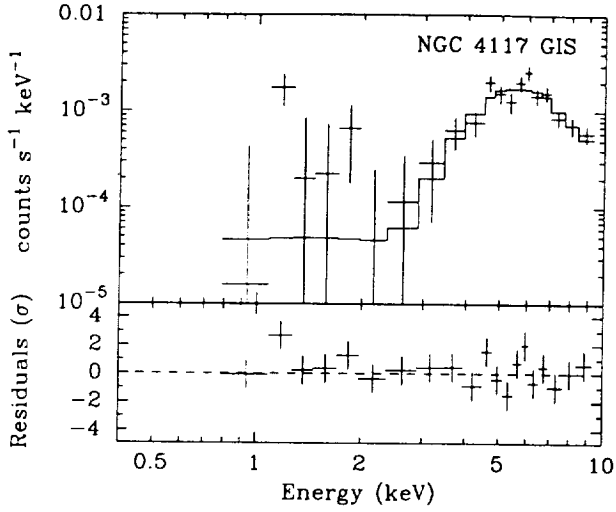
Fig. 4.— GIS spectrum of NGC 4117. Crosses are the observed data and histograms are the best-fit absorbed power-law model.
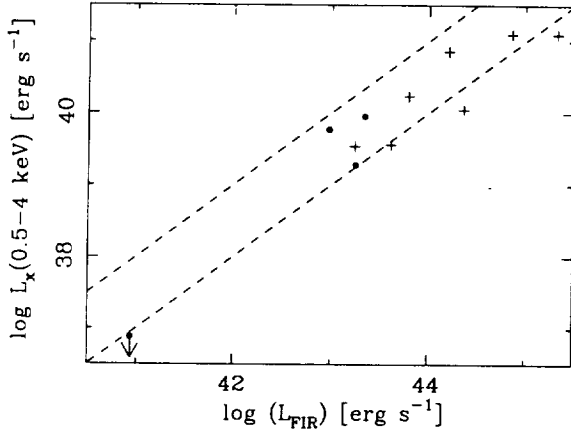

Fig. 5.— Correlation between soft X-ray luminosity and fir infrared luminosity for type 2 LINERs (filled circles) and starburst galaxies (crosses). The soft X-ray luminosities are the Raymond-Smith component of a two component spectral fit to the *ASCA* data except for NGC 404 and NGC 4192. Dashed lines correspond to $\log L_X / L_{FIR} = -3$ (upper) and -4 (lower). Starburst galaxy sample consists of NGC 5236 (M83), NGC 253, NGC 3310, NGC 3034(M82), NGC 2146, NGC 3256, and NGC 3690 (from left to right in the plot).